Magnetic structure of hexagonal $R\mathrm{MnO_3}$ (R=Y, Sc): Thermal evolution from neutron powder diffraction data

A. Muñoz*
Departamento de Física, EPS, Universidad de Carlos III, Avenida de la Universidad 30, Leganés, E-28911 Madrid, Spain

J. A. Alonso, M. J. Martínez-Lope, M. T. Casáis, and J. L. Martínez
Instituto de Ciencia de Materiales de Madrid, CSIC, Cantoblanco, E-28049 Madrid, Spain

M. T. Fernández-Díaz
Institut Laue-Langevin, Boîte Postale 156X, 38042 Grenoble Cèdex 9, France
(Received 31 March 2000)

The magnetic structures of the hexagonal $\mathrm{YMnO_3}$ and $\mathrm{ScMnO_3}$ oxides (space group $P6_3cm$) have been studied by neutron-diffraction experiments on powder samples. This study has been complemented with magnetic susceptibility and specific-heat measurements. They confirm that $\mathrm{YMnO_3}$ and $\mathrm{ScMnO_3}$ become ordered below $T_N \approx 70$ K and $T_N \approx 129$ K, respectively, according to a triangular antiferromagnetic structure. The latter compound undergoes a second magnetic transition below 75 K, corresponding to a spin reorientation. The presence of weak ferromagnetism of Dzialoshinskii-Moriya type is observed in all the ordered region for the Sc material. In both compounds the moments are contained in the (a,b) plane and oriented perpendicular (R=Y) or parallel (R=Sc) to the [100] directions. The low-temperature ordered moments are $2.90(2)\mu_B$ (R=Y) and $3.54(3)\mu_B$ (R=Sc) at T=1.7 K. The different behavior observed in the thermal evolution of the magnetic structure of both compounds is discussed in terms of geometrical parameters determined from high-resolution structural data. The origin of the weak ferromagnetism in $\mathrm{ScMnO_3}$ is also analyzed.

I. INTRODUCTION

$R\mathrm{MnO_3}$ rare-earth manganites form an interesting family showing a wide variety of physical properties. For R^{3+} cations with large ionic size, $R\mathrm{MnO_3}$ oxides crystallize in a perovskite-type structure, with orthorhombic symmetry (space group *Pbnm*).[1] When hole doped by partially replacing R^{3+} by A^{2+} cations (A=Ca, Sr, Ba), these perovskites are well known to display colossal magnetoresistance properties.[2] For rare-earth cations smaller than Tb^{3+} (R=Ho, Er, Tm, Yb, Lu) as well as Y^{3+} and Sc^{3+}, the perovskite structure becomes metastable and a new hexagonal polytype stabilizes (space group $P6_3cm$).[3] In the hexagonal phase, a ferroelectric behavior has been described to coexist with magnetic ordering at low temperature. The ferroelectricity in hexagonal $R\mathrm{MnO_3}$ was discovered by Bertaut, Forrat, and Fang in 1963.[4] Recently, thin films of these compounds have been proposed for nonvolatile memory devices. In particular, $Y\mathrm{MnO_3}$ thin films have been grown.[5] Anomalies in the dielectric constant observed in $\mathrm{YMnO_3}$ near its Néel temperature indicate a coupling between the ferroelectric and the magnetic ordering.[6] For a better understanding of this coupling a thorough study of the variations of Raman and IR phonon spectra with magnetic and ferroelectric orderings have been recently carried out.[7]

In the hexagonal phase of $R\mathrm{MnO_3}$ there are six formula units per unit cell. The six Mn atoms are distributed in the $z=0$ and $z=\frac{1}{2}$ planes. In the zero plane the Mn atoms are placed along the axes $\boldsymbol{a_1}$, $\boldsymbol{a_2}$, and $-(\boldsymbol{a_1}+\boldsymbol{a_2})$ and, in the $z=\frac{1}{2}$ plane along the axes $-\boldsymbol{a_1}$, $-\boldsymbol{a_2}$ and $(\boldsymbol{a_1}+\boldsymbol{a_2})$. Each Mn atom occupies the center of a triangular bipyramid whose vertices are oxygen atoms. The magnetic structure of these compounds were studied by Bertaut and co-workers[8,9] and Koehler *et al.*[10] a long time ago. According to the microscopic method developed by Bertaut[11] four different spin configurations are possible for these compounds. Two of them correspond to a uniaxial spin configuration; in one case it is ferromagnetic and in the other case antiferromagnetic, for which the moments alternate in sign from the $z=0$ to the $z=\frac{1}{2}$ layer. The other two configurations involve a triangular arrangement with the moments in the basal plane, being the coupling between the $z=0$ and the $z=\frac{1}{2}$ layers ferromagnetic in one case and antiferromagnetic in the other case. For most of the $R\mathrm{MnO_3}$ compounds (R=Lu, Tm, Er, Ho, Sc, and Y) it was established that the magnetic moments of the Mn atoms order according to a triangular structure[8–10] although it could not be established whether the coupling between the $z=0$ and $z=\frac{1}{2}$ layers is ferromagnetic or antiferromagnetic, because the x parameter for Mn atoms is very close to $\frac{1}{3}$ and both models give rise to very similar magnetic intensities. In the present paper a study of the magnetic ordering of $\mathrm{YMnO_3}$ and $\mathrm{ScMnO_3}$ has been carried out. The possible magnetic structures have been obtained by using the group theory analysis; the complement of some macroscopic measurements (magnetization, susceptibility, and specific heat) allowed us to solve the indetermination of precedent papers, giving the orientation of the magnetic moments relative to the unit cell. The crystallographic structure of both compounds has also been refined from high-resolution neutron powder-diffraction data. The thermal evolution of the mag-

netic structures for both compounds is described and analyzed.

II. EXPERIMENT

A. Sample preparation

Hexagonal $R\mathrm{MnO_3}$ polycrystalline phases were prepared from citrate precursors obtained by soft chemistry procedures. Stoichiometric amounts of analytical grade R_2O_3 (R = Sc, Y) and $MnCO_3$ were dissolved in citric acid, by adding several droplets of concentrated HNO_3 to favor the solution of R_2O_3 oxides. The citrate+nitrate solutions were slowly evaporated, leading to organic resins containing a random distribution of the involved cations at an atomic level. These resins were first dried at 120 °C and then slowly decomposed by heating at temperatures up to 700 °C in air. This treatment gave rise to highly reactive precursor materials, amorphous to x-ray diffraction. The precursor powders were finally heated at 1150 °C (R=Sc) or 1000 °C (R=Y) in air for 12 h, thus obtaining well crystallized powders.

B. Experimental measurements

Magnetic measurements were perfomed in a commercial superconducting quantum interference device (SQUID) magnetometer. The magnetic susceptibility was measured in a magnetic field $H=5$ kOe and in the temperature ranges $2<T<300$ K and $2<T<400$ K for $YMnO_3$ and $ScMnO_3$, respectively. Magnetization measurements were carried out at different temperatures and in magnetic fields up to 50 kOe.

The specific heat was measured in a semiadiabatic He calorimeter using the heat-pulsed method from $T=2$ up to 100 K and in fields up to 90 kOe.

Neutron powder-diffraction (NPD) diagrams were collected at the Institut Laue-Langevin in Grenoble (France). High-resolution NPD data were acquired to refine the crystallographic structures at room temperature (RT); for $ScMnO_3$ at D2B difractometer with $\lambda=1.594$ Å, and for $YMnO_3$ at D20 difractometer with $\lambda=1.30$ Å. The thermal evolution of the NPD patterns for both compounds was followed at D20 with a longer wavelength, $\lambda=2.413$ Å, in the temperature range 2–150 K. All data were analyzed using the Rietveld method[12] and the refinement of both crystal and magnetic structures were carried out with the program FULLPROF.[13] In the refinements the peak shape was described by a pseudo-Voigt function for those NPD recorded on the high-resolution powder diffractometer and by a Gaussian function in the case of the patterns recorded with $\lambda=2.413$ Å. The background was fitted either with a fifth-degree polynomial function or by interpolation between regions devoid of Bragg reflections. The Fermi scattering lengths were for Y, Sc, Mn, and O, respectively, 7.750, 12.300, −3.730, and 5.830 fm. The magnetic form factor used for Mn atoms was determined with the coefficients taken from the International Tables[14] for the spin only, $\langle j_0 \rangle$.

III. RESULTS

A. Magnetic measurements

The magnetic susceptibilities of $YMnO_3$ and $ScMnO_3$ are presented in Figs. 1 and 2, respectively. The reciprocal susceptibility has a linear dependence above 200 K for $YMnO_3$ and above 325 K for $ScMnO_3$. This reveals a Curie-Weiss behavior, being the effective paramagnetic moment $4.4(1)\mu_B$ and $4.6(1)\mu_B$ for $YMnO_3$ and $ScMnO_3$, respectively. These values are close to the free Mn^{3+} ion value, $4.9\mu_B$ (for the spin only $S=2$). The extrapolated paramagnetic temperatures are −312 K for $YMnO_3$ and −663 K for $ScMnO_3$. In the magnetic susceptibility of $YMnO_3$ no anomalies are observed, although there is a notable increase below 100 K. As for $ScMnO_3$, the magnetic susceptibility shows a quite different pattern of behavior. In the zero-field-cooled measurements, an anomaly is observed at around 129 K (better observed in the reciprocal susceptibility curve), revealing the onset of a magnetic ordering; on the other hand, the susceptibility undergoes an abrupt increase below 50 K, reaching a maximum value at around 37 K and decreasing for lower temperatures. In the field-cooled measurements, the susceptibility at first experiences an important enhancement below 130 K; below 50 K it undergoes an abrupt increase tending towards a saturation value. This indicates the presence of a weak ferromagnetism effect.

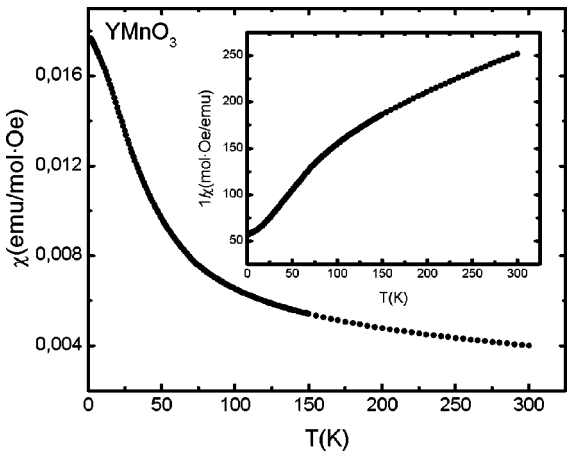

FIG. 1. Thermal variation of the magnetic susceptibility of $YMnO_3$ measured in field-cooled (FC) conditions under $H=5$ kOe. Inset: reciprocal susceptibility versus temperature.

The isothermal magnetization curves for $YMnO_3$ and $ScMnO_3$ are presented in Figs. 3 and 4, respectively. For $YMnO_3$ the magnetization curves do not present neither

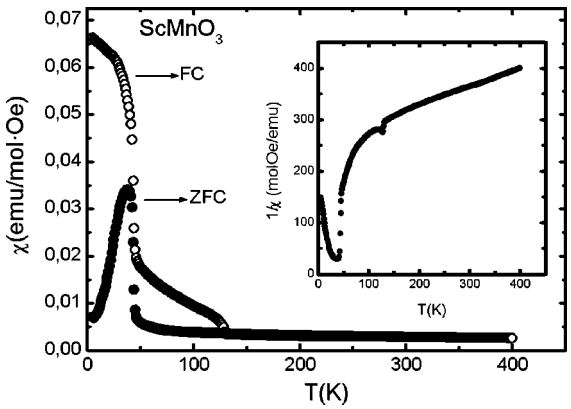

FIG. 2. Magnetic susceptibility for $ScMnO_3$ in zero-field-cooled (ZFC) and in field-cooled (FC) conditions ($H=0.5$ kOe). Inset: reciprocal susceptibility vs temperature.

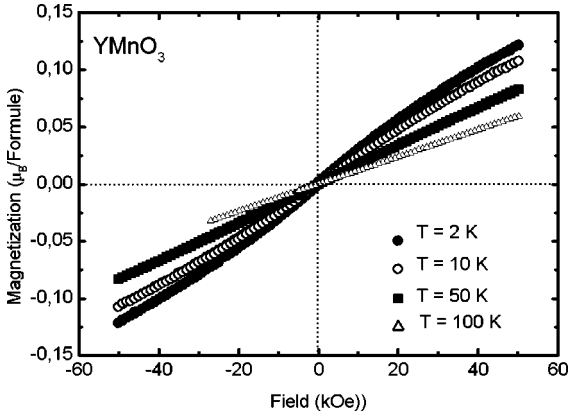

FIG. 3. Magnetization isotherms for $YMnO_3$.

spontaneous magnetization nor hysteresis phenomenon and the 50-kOe magnetic field is too low to saturate the magnetization. For $ScMnO_3$, the magnetization curves exhibit a hysteresis for fields from -15 to 15 kOe, which decreases as temperature increases. Although at $T = 2$ K the magnetic moments start to reorient at 3 kOe, the final magnetic field, 50 kOe is too low to complete the reorientation. At this temperature, the spontaneous magnetization is $0.009\mu_B/Mn^{3+}$, very small compared with the theoretical saturation value of $4\mu_B$ (for the spin only). As it is shown in the inset of Fig. 4, under a magnetic field a spontaneous magnetization is observed in the whole ordered region. This implies that the weak ferromagnetism is present below the onset of the magnetic ordering.

B. Specific heat

The specific-heat data for $YMnO_3$ and $ScMnO_3$ in different magnetic fields are plotted in Figs. 5(a) and 5(b), respectively. A calculation of the magnetic contribution to the heat capacity around the magnetic transitions is also shown (insets in Figs. 5(a) and 5(b)). The nonmagnetic contribution has been calculated by an extrapolation method. In the temperature range 70–260 K, the lattice specific heat has been obtained by following the Einstein model with three oscillators centered at $T=240$, 500, and 800 K. Below 70 K, after excluding the regions around the magnetic transitions, the specific-heat has been simulated by assumming a linear dependence of C_P/T with temperature. In the specific-heat

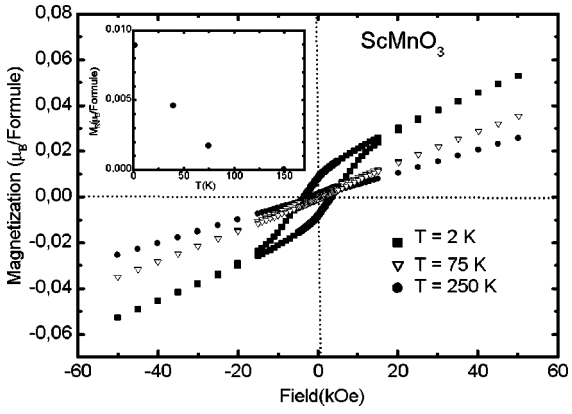

FIG. 4. Magnetization isotherms for $ScMnO_3$.

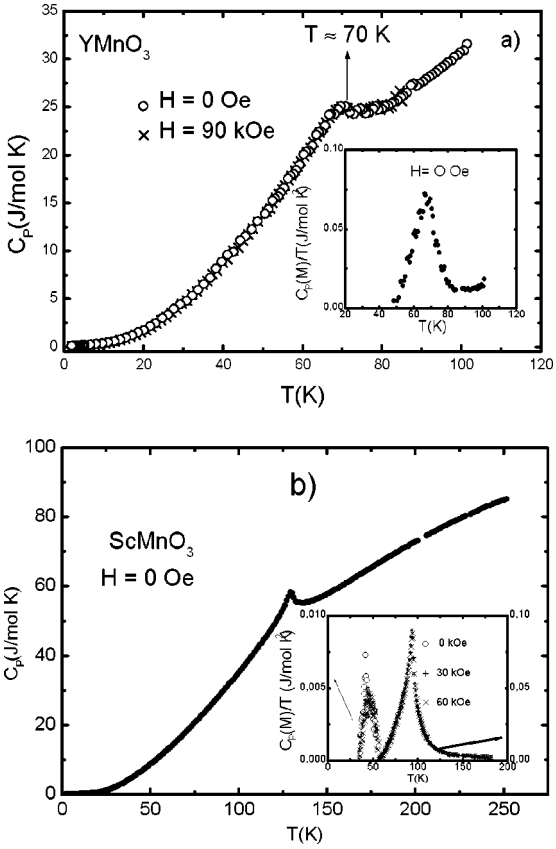

FIG. 5. Specific heat versus temperature. Inset: magnetic contribution to the specific heat around the magnetic transitions. (a) For $YMnO_3$ in $H=0$ and 90 kOe. (b) For $ScMnO_3$ in $H=0$, 30, and 60 kOe.

curves measured in zero field sharp anomalies are observed at $T\approx 70$ K for $YMnO_3$ and at $T\approx 129$ K for $ScMnO_3$, indicating the onset of a magnetic ordering. For $ScMnO_3$ another small anomaly takes place at around $T\approx 43$ K, which is better observed in the magnetic heat capacity [inset in Fig. 5(b)]. This reveals the transition to another magnetic phase, in good agreement with the susceptibility measurements. When a magnetic field is applied no appreciable changes are observed in the specific heat of $YMnO_3$ and $ScMnO_3$. No shifts appear in the transitions at $T\approx 70$ K for $YMnO_3$ and at $T\approx 129$ K for $ScMnO_3$. Only for $ScMnO_3$, in the transition observed at $T\approx 43$ K, a slight shift to higher temperatures is observed. The entropy gain in the magnetic transition has been calculated from the magnetic contribution to the specific heat. In zero magnetic field it results in $\Delta S=0.15$ R for $YMnO_3$ and $\Delta S=0.35$ and 0.07 R for $ScMnO_3$ in the transition corresponding to $T\approx 129$ K and $T\approx 43$ K, respectively. In $ScMnO_3$, the great difference in the entropy gain between both magnetic transitions probably indicates that the transition observed at $T\approx 43$ K is a first-order one, whereas the transition at $T\approx 129$ K is second order.

C. Crystal structure

The $YMnO_3$ crystal structure was refined from NPD data collected in the paramagnetic region at room temperature, $\lambda=1.30$ Å. All the reflections were indexed in the hexagonal space group $P6_3cm$ with the lattice parameters a

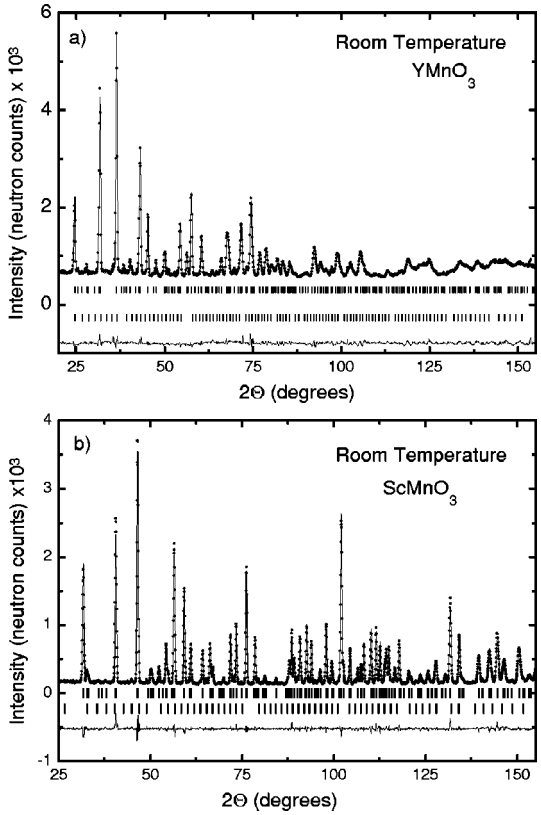

FIG. 6. Observed (●) and calculated (—) neutron-diffraction pattern for RMnO$_3$ at room temperature. Bragg reflections are indicated by tic marks: the first series corresponds to RMnO$_3$ and the second row to the minor impurity phase R_2O_3. The difference between the observed and calculated pattern is plotted at the bottom. (a) For YMnO$_3$. (b) For ScMnO$_3$.

$=6.1553(3)$ Å and $c=11.4026(8)$ Å. The goodness of the fit is illustrated in Fig. 6(a), showing an excellent agreement between observed and calculated pattern. The most relevant crystallographic parameters are included in Table I. Some selected bonding distances and angles are also listed (see Table II). The crystal structure of ScMnO$_3$ was refined from high-resolution NPD data collected at room temperature and at $\lambda=1.594$ Å. The quality of the fit is shown in Fig. 6(b). The crystallographic parameters listed in Tables I and II are in good agreement with those recently reported,[15] obtained from single-crystal x-ray diffraction. In both patterns some minor impurities of R_2O_3 (R=Y, Sc) were detected, and were included as secondary phases in the final refinement (2% Y_2O_3, 2% Sc_2O_3).

As it is shown in Fig. 7 each Mn atom is coordinated by five oxygen atoms in a bypyramidal configuration. One O(3) atom and two O(4) atoms are in the equatorial plane of the bypyramid, whereas the O(1) and O(2) atoms are at the apexes. Y(Sc) atoms occupy two crystallographic positions, $R(1)$ and $R(2)$, both of them bonded to seven oxygen atoms. Both RO_7 polyhedra can be described as monocapped octahedra. The capping oxygens are O(3) for $R(1)$ and O(4) for $R(2)$. Along the z axis, the structure consists of layers of corner-sharing MnO_5 bypiramids separated by layers of edge-sharing RO_7 polyhedra. According to Table II, smaller unit-cell parameters are observed for ScMnO$_3$, and the average Mn-O distances in MnO_5 units are significantly shorter

TABLE I. Structural parameters after the Rietveld refinement of NPD for RMnO$_3$ (R=Y, Sc) at room temperature. Atomic positions: $R1$ and O3 at 2a (0,0,z); $R2$ and O4 at 4b ($\frac{1}{3},\frac{2}{3},z$); Mn, O1, and O2 at 6c (x,0,z) for Mn $z=0$.

		YMnO$_3$	ScMnO$_3$
a (Å)		6.1553(3)	5.83338(4)
c (Å)		11.4026(8)	11.16862(9)
V (Å^3)		374.15(3)	329.132(4)
Impurity		Y_2O_3=1.7(2)%	Sc_2O_3=2.1(1)%
Atoms			
$R1$	z	0.2689(14)	0.2747(7)
	B_{iso} (Å^2)	0.53(4)	0.50(1)
$R2$	z	0.2290(10)	0.2308(6)
	B_{iso} (Å^2)	0.53(4)	0.50(1)
Mn	x	0.3208(18)	0.3316(15)
	B_{iso} (Å^2)	0.20(20)	0.20(3)
O1	x	0.3100(11)	0.3018(3)
	z	0.1621(13)	0.1680(6)
	B_{iso} (Å^2)	0.43(4)	0.20(2)
O2	x	0.6389(9)	0.6357(3)
	z	0.3367(13)	0.3329(6)
	B_{iso} (Å^2)	0.43(4)	0.20(2)
O3	z	0.4745(17)	0.4678(8)
	B_{iso} (Å^2)	0.87(5)	0.19(2)
O4	z	0.0133(5)	0.0238(6)
	B_{iso} (Å^2)	0.87(5)	0.19(2)
Discrepancy factors			
χ^2		1.0	2.5
R_p(%)		2.7	4.0
R_{wp}(%)		3.5	5.1
R_B(%)		4.2	2.7

in ScMnO$_3$, which will play an important role in the different magnetic structures observed in both compounds. Mn-O bond lengths are in agreement with the sum of the ionic radii. Moreover, in the RO_7 polyhedron, the Y-O distances are larger than Sc-O bond lengths, as expected for the larger size of Y^{3+}. Also, the average R-O distances are close to the sum of the ionic radii.

D. Magnetic structure

1. $YMnO_3$

Figure 8(a) displays the thermal evolution of the neutron diffraction patterns correspondig to YMnO$_3$. Below 77 K an increase in the intensity of some Bragg reflections is observed. On the other hand, new peaks appear on Bragg positions forbidden by the space group $P6_3cm$, in particular reflections (h,0,l) with odd l. This confirms the existence of a magnetic ordering below T_N characterized by a magnetic unit cell which coincides with the chemical unit cell (propagation vector $\boldsymbol{k}=0$). As temperature decreases the intensity of the magnetic reflections smoothly increase, reaching a constant value at low temperature, suggesting that the magnetic structure remains stable in all the temperature range.

TABLE II. Selected bond distances and bond angles for $R\mathrm{MnO_3}$ (R=Y, Sc).

Atoms	$Y\mathrm{MnO_3}$ (Å)	$\mathrm{ScMnO_3}$ (Å)
Mn−O1	1.850(15)	1.884(7)
Mn-O2	1.878(15)	1.876(7)
Mn-O3	1.996(11)	1.968(9)
Mn-O4($X2$)	2.097(6)	1.967(5)
⟨Mn-O⟩	1.98(2)	1.932(3)
ΣRadii	1.949	1.949
$R1-O1(X3)$	2.263(13)	2.126(6)
$R1-O2(X3)$	2.353(9)	2.223(3)
$R1-O3$	2.345(25)	2.157(12)
$R2-O1(X3)$	2.260(7)	2.160(3)
$R2-O2(X3)$	2.323(11)	2.182(5)
$R2-O4$	2.459(19)	2.312(10)
$\langle R1-O1,O2\rangle$	2.308(16)	2.179(6)
$\langle R2-O1,O2\rangle$	2.291(13)	2.171(6)
ΣRadii	2.327	2.162
Angle(°)		
O1-Mn-O2	174.5(9)	179.5(7)
O1-Mn-O3	96.3(9)	95.2(5)
O4-Mn-O4	115.9(2)	117.7(2)
O2-Mn-O4	90.1(8)	94.8(4)
O3-Mn-O4	122.1(4)	121.1(3)
O2-Mn-O3	89.2(8)	85.3(4)
O1-Mn-O4	86.9(7)	84.9(4)
Mn-O3-Mn	117.9(8)	116.7(6)
Mn-O4-Mn	119.5(7)	118.2(6)
R1−O1-Mn	124.6(9)	123.8(4)
R2−O2-Mn	124.9(7)	123.8(4)

A neutron-diffraction pattern collected at 1.7 K was used to determine the magnetic structure. After checking all of the possible magnetic modes obtained in the Appendix, the best agreement with the experimental data was obtained for the magnetic structure given by the basis vectors of the irreducible representation Γ_1. In Fig. 9(a) the observed and calculated NPD patterns are presented. The value of the magnetic moment for each Mn atom after the refinement at $T=1.7$ K is $2.90(2)\mu_B$ (see Table III), somewhat smaller than that expected for spin only Mn^{3+} cations, $4\mu_B$. The magnetic structure associated to the irreducible representation Γ_3, but with $m_z=0$, could also be an acceptable model as it was pointed out by Bertaut;[9] however, the agreement factors are significantly worse. For instance, the magnetic R_{MAG} factor for Γ_3 is 10.8% versus $R_{MAG}=7.6\%$ for the solution associated to Γ_1 (see Table III).

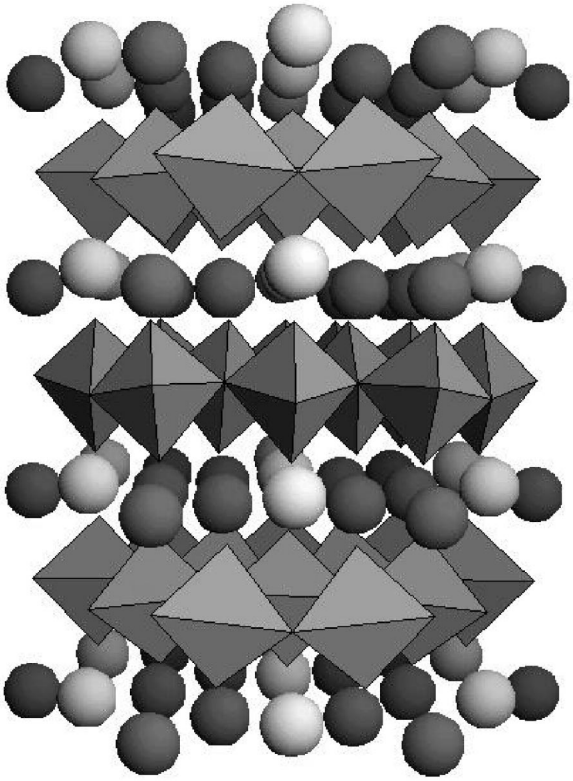

FIG. 7. Schematic representation of the crystallographic structure of $R\mathrm{MnO_3}$ (R=Y, Sc). Mn is located at the center of the polyhedra, $R1$ at 2a (0,0,z), and $R2$ at 4b ($\frac{1}{3},\frac{2}{3},z$) are represented by open and solid circles, respectively.

In Fig. 10(a), a view of the magnetic structure associated to Γ_1 is presented. The spins of the layers $z=0$ and $z=\frac{1}{2}$ are antiferromagnetically coupled. In each layer, the spin ar-

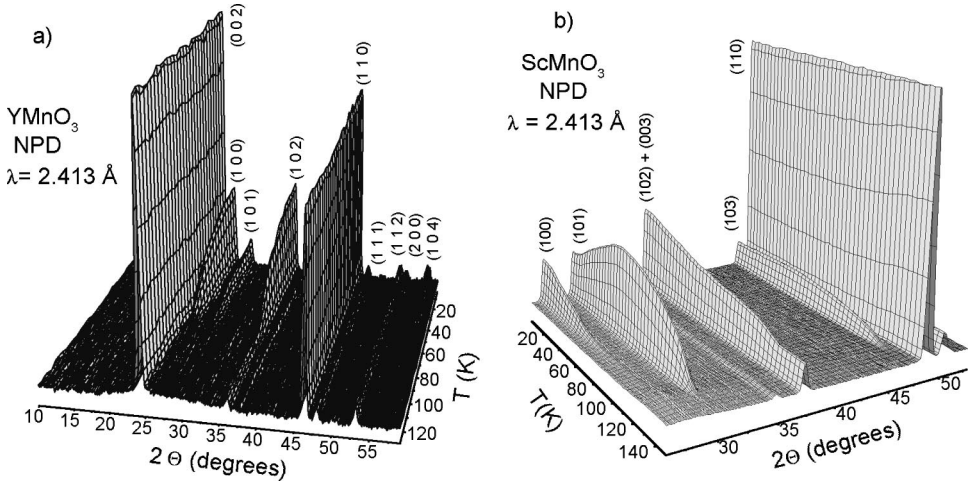

FIG. 8. Evolution of the neutron-diffraction patterns with temperature. (a) For $YMnO_3$ in temperature range 2.5–127 K. (b) For $ScMnO_3$ in the temperature range 1.8–147 K.

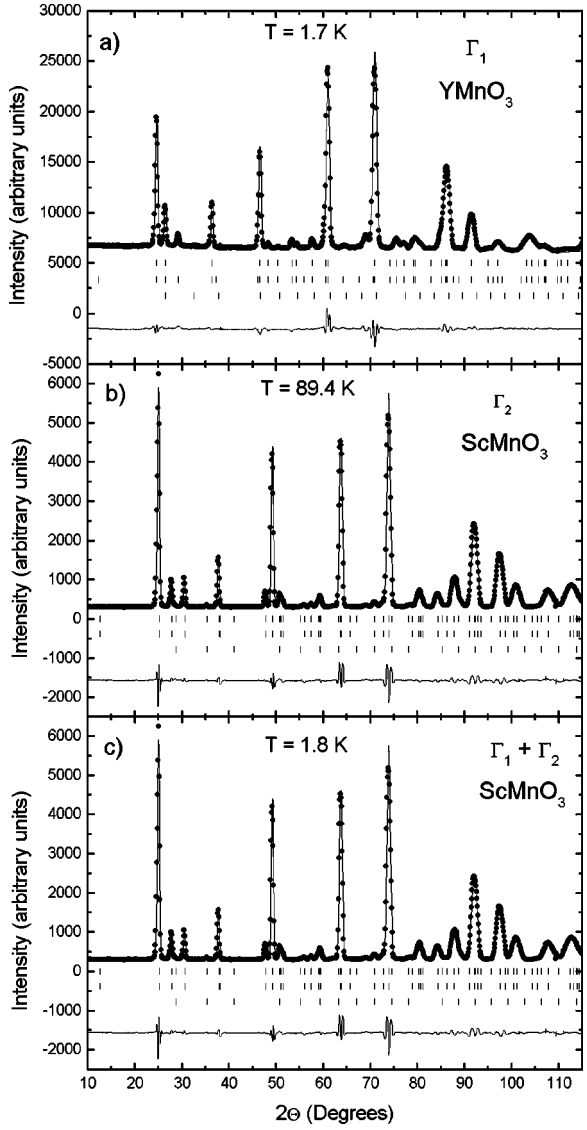

FIG. 9. Observed (●) and calculated (—) neutron-diffraction pattern after the magnetic structure refinement. (a) For $YMnO_3$ at $T=1.7$ K; (b) and (c) for $ScMnO_3$ at $T=89.4$ K and $T=1.8$ K.

rangement is triangular with the magnetic moments perpendicular to the axis along which the Mn^{3+} cations are placed. The analysis of the NPD patterns collected at different temperatures allowed us to follow the thermal evolution of the Mn magnetic moment. As it is shown in Fig. 11(a), the magnetic moment increases as temperature decreases, reaching saturation below 8 K. The thermal evolution of the lattice parameters is shown in Figs. 12(a) and 12(b). The a and c unit-cell parameters present a different thermal behavior, and remain constant below 40 K.

TABLE III. Results of the magnetic structure refinement of RMnO$_3$ (R=Mn, Sc): magnetic ordering, magnetic moment values and agreement factors.

Temperature	$YMnO_3$ 1.7 K	$ScMnO_3$ 89.4 K	$ScMnO_3$ 1.8 K
Structure	Γ_1	Γ_2	$\Gamma_1+\Gamma_2$
m_T(Mn)	$2.90(2)\mu_B$	$3.03(3)\mu_B$	$3.54(3)\mu_B$
Angle Mn(1) with $\boldsymbol{e}_x$	90°	0°	54(1)°
R_N(%)	3.7	2.8	2.7
R_{MAG}(%)	7.6	4.6	6.3
χ^2	2.5	2.3	2.3

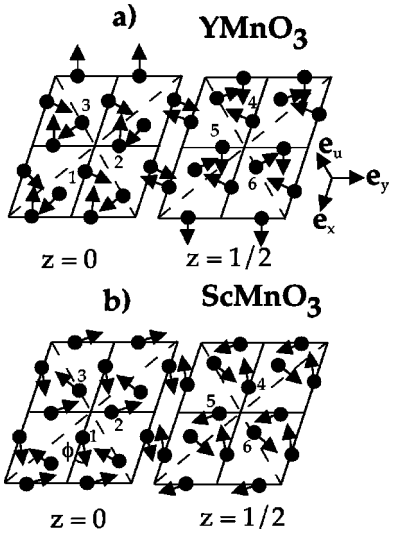

FIG. 10. Schematic representation of the magnetic structure of RMnO$_3$. Only the Mn atoms are plotted. (a) For $R=$Y; (b) for $R=$Sc, $\phi=0°$ for $75<T<130$ K and $17°<\phi<54°$ for $1.8<T<75$ K. Mn atoms: 1 $(x,0,0)$, 2 $(0,x,0)$, 3 $(-x,-x,0)$, 4 $(-x,0,\frac{1}{2})$, 5 $(0,-x,\frac{1}{2})$, and 6 $(x,x,\frac{1}{2})$.

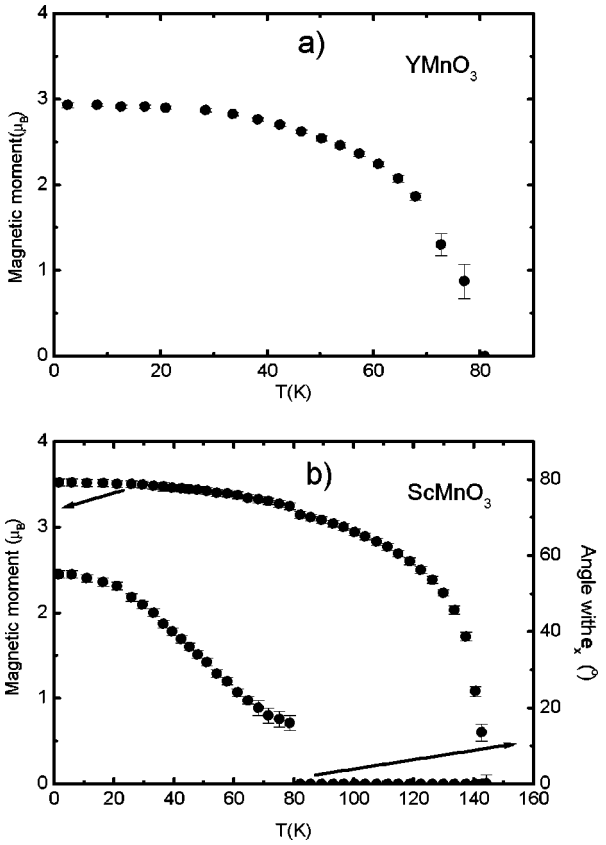

FIG. 11. (a) Thermal evolution of the Mn^{3+} magnetic moment of $YMnO_3$. (b) Themal evolution of the magnetic moment and of the ϕ angle with the [100] axis for $ScMnO_3$.

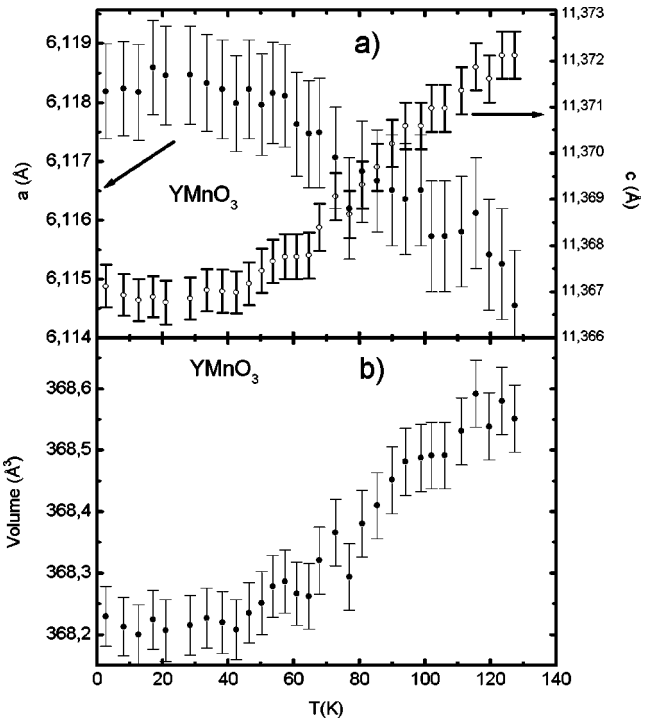

FIG. 12. Thermal evolution of the lattice parameters for $YMnO_3$: (a) **a** and **c** and (b) cell volume.

2. $ScMnO_3$

The thermal evolution of the NPD patterns corresponding to $ScMnO_3$ is shown in Fig. 8(b). Below 140 K $(h,0,l)$, reflections with l odd, forbidden by the space-group symmetry, are observed; some permitted reflections, in particular $(h,0,l)$ with l even, increase their intensity. Note that the (1,0,0) reflection is not observed. This, in agreement with the magnetic measurements, confirms the appearance of a magnetic ordering, which is characterized by the propagation vector $\boldsymbol{k}=0$. As shown in Fig. 8(b), important changes in the intensity of some reflections take place below 75 K: the (1,0,0) reflection starts to be observed and, at the same time, the intensity of the (1,0,1) reflection begins to decrease. This suggests a transition to a different magnetic arrangement, also characterized by a propagation vector $\boldsymbol{k}=0$.

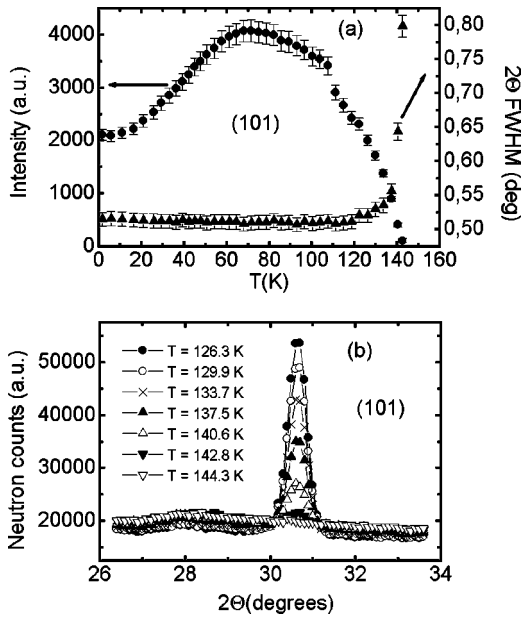

FIG. 13. Thermal evolution of the magnetic peak (101). (a) Intengrated intensity and linewidth. (b) NPD pattern around the peak.

On comparing the specific-heat measurements and the thermal evolution of the NPD patterns, a small discrepancy on the ordering temperature is appreciated. It can be seen in Figs. 13(a) and (b) that the magnetic reflection (101) starts to be observed at around 140 K, above the ordering temperature $T_N \approx 129$ K deduced from the specific-heat curve. This is very probably due to the presence of a low-dimensional short-range order, as it was pointed out by M. Bieringer *et al.*[16] To investigate this point, the thermal evolution of the linewidth full width at half maximum of some magnetic peaks has been analyzed. In particular, the linewidth of the (101) magnetic peak, that remains nearly constant below 129 K, experiences an important increase above T_N, that indicates the existence of a short-range order.

For the first magnetic phase observed immediately below T_N, after considering all the solutions given in the Appendix, only two of them are compatible with the experimental data, those associated to Γ_2 and Γ_4. However, as it is pointed out in the Appendix, only Γ_2 is compatible with the existence of a weak ferromagnetism. Therefore, in order to account for the magnetic measurements, the solution Γ_2 is selected. It implies a triangular spin arrangement where the magnetic moment of the Mn atoms are parallel to the [110] axis, within each (a,b) layer. The $z=0$ and $z=\frac{1}{2}$ layers are antiferromagnetically coupled. At $T=89.4$ K the magnetic moment value is $3.03(3)\mu_B$ (see Table III). Although the solution permits a ferromagnetic component in the magnetic moment along the z direction, m_z, the refinement of the NPD patterns collected in this region shows that $m_z=0$.

In the second transition, around 75 K, there is a change in the spin orientation of the moments within the (a,b) plane. In a first trial, we considered that the magnetic structure is given by the basis vectors of only one irreducible representation, in the temperature range 75–1.8 K: the experimental data could not be satisfactorily fitted for any of the different magnetic modes presented in Table V. However, if it is assumed that the $z=0$ and $z=\frac{1}{2}$ layers are still antiferromagnetically coupled, a solution is possible. In this solution the magnetic moment of the Mn(1) atom, position $(x,0,0)$, forms a variable angle ϕ with the $\boldsymbol{e}_x$ axis. The orientation of the moments of the Mn(2) atom, position $(0,x,0)$ and Mn(3), position $(-x,-x,0)$, are obtained by rotating 120° and $-120°$, respectively, the magnetic moment of the Mn(1) atom around the z axis. In fact, this means that the spin arrangement is given in terms of the basis vectors of two irreducible representations Γ_1 and Γ_2. From the fitting, an increase of the ϕ angle from $\phi=17(2)°$ at $T=75$ K to $\phi=54(1)°$ at $T=1.8$ K is observed (see Fig. 11(b)). The value of the magnetic moment simultaneously increases, reaching $3.54(3)\mu_B$ at T = 1.8 K. The corresponding magnetic structure is presented in Fig. 10(b). In Figs. 9(b) and 9(c) the observed and calculated pattern in the magnetic structure determination at $T=89.4$ K and $T=1.8$ K are presented. The corresponding agreement factors are included in Table III. In

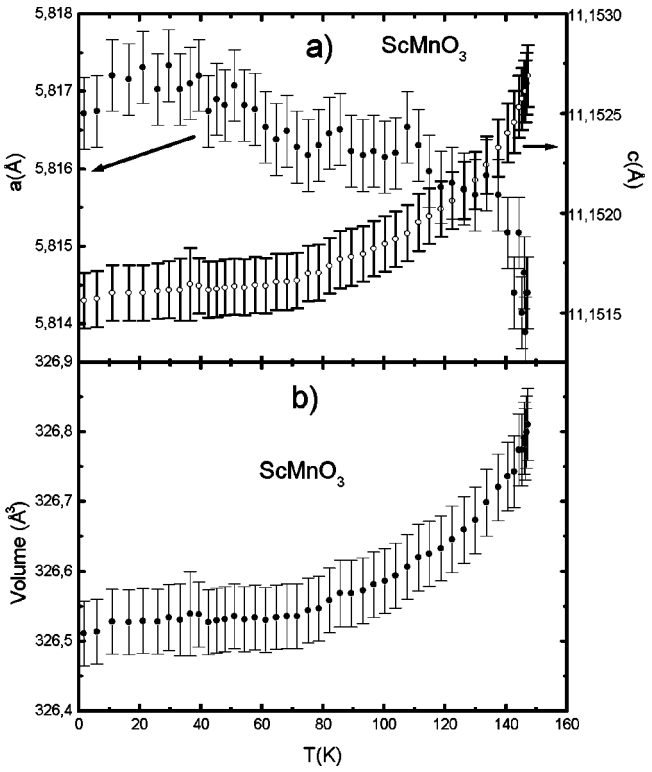

FIG. 14. Thermal evolution of the lattice parameters for $ScMnO_3$: (a) **a** and **c** and (b) cell volume.

this temperature range, the inclusion of a ferromagnetic component along the z direction was also checked, but it was obtained a value for m_z close to zero. Figures 14(a) and (b) illustrate the thermal evolution of the lattice parameters. The c lattice parameter undergoes an important change in the variation regime after the first magnetic transition T_N and afterwards it decreases very slowly as temperature decreases. On the other hand, the a parameter decreases below the first ordered region down to 75 K, when the second magnetic transition takes place, and then its value remains nearly constant. The cell volume presents a thermal evolution similar to that of the a parameter. Finally, let us point out that one of the solutions associated to the irreducible representation Γ_6 is also compatible with the experimental results in all the temperature range. In particular, a solution with equal moments for all the atoms and with the spins placed in the (a,b) plane. For this solution, the orientation of the moments of the Mn(2) and Mn(3) atoms are obtained by rotating $-120°$ and 120°, respectively, the moment of the Mn(1) atom. The orientation of the magnetic moment of the Mn(1) atom would form a variable angle with the $\boldsymbol{e}_x$ axis. Nevertheless, this solution must be discarded since it is not compatible with weak ferromagnetism from symmetry considerations, as it is indicated in the Appendix.

IV. DISCUSSION

Susceptibility measurements show that $ScMnO_3$ become magnetically ordered below $T_N \approx 129$ K, and the magnetic arrangement undergoes a change below 50 K. This is confirmed by specific-heat measurements since two anomalies are observed at 129 and 43 K. The hysteresis observed in the zero-field-cooled and in the field-cooled susceptibility curves suggests the presence of a weak ferromagnetism effect. This is also confirmed by the isothermal magnetization curves, in which a remnant magnetization appears in the ordered region. All these results are in good agreement with those recently reported by Bieringer *et al.*[16] and Xu *et al.*[17] Regarding $YMnO_3$, although no anomalies are observed in the susceptibility plots, the presence of a peak in the specific-heat curve indicates the onset of antiferromagnetic ordering at $T_N \approx 70$ K, what is confirmed by neutron-diffraction measurements.

In $R\mathrm{MnO_3}$ compounds the magnetic interactions among the Mn atoms are the superexchange interactions via Mn-O-Mn bonds. In the plane perpendicular to the sixfold axis the exchange paths for the first and second nearest neighbors are Mn-O(3)-Mn and Mn-O(4)-Mn, respectively. The Mn-O distances are shorter for $ScMnO_3$, which involves stronger exhange interactions. This accounts for the fact that $ScMnO_3$ becomes ordered at a higher temperature than $YMnO_3$.

Neutron-diffraction experiments have shown that the magnetic structures exhibited by both compounds present similar features, in both cases the magnetic moments are contained in the plane perpendicular to the sixfold axis and the spin arrangement is triangular. Besides, in both compounds the coupling between the z layers is antiferromagnetic. However, important differences are found in the magnetic behavior of both compounds. First, magnetization measurements reveal the presence of a spontaneous magnetization in $ScMnO_3$. This low spontaneous magnetization ($0.009\mu_B$/Mn at $T=2$ K) can be ascribed to a weak ferromagnetic interaction of Dzialoshinskii-Moriya type.[18] An alternative would be the existence of a ferromagnetic double exchange interaction, between Mn^{3+} and Mn^{4+} cations. The necessary Mn^{4+} content for this interaction to take place would imply the presence of cation vacancies (either at the R or the Mn sublattices), which have not been observed from the high-resolution structural analysis. Moreover, the symmetry of the magnetic structure found by neutron-diffraction measurements is compatible with that type of weak ferromagnetism; in particular, a ferromagnetic component along the z direction is permitted.

It is worth underlining the differences observed in the magnetic structures exhibited by both compounds. Concerning the orientation of the magnetic moments in the basal plane, for $YMnO_3$ the spins are oriented parallel to the [120] directions, whereas for $ScMnO_3$ they are initially lying along the [100] direction, and below 75 K they rotate in the (a,b) plane. Concerning the magnitude of the ordered moments at low temperature, the observed value for $YMnO_3$, $2.90(2)\mu_B$, is significantly smaller than that for $ScMnO_3$, $3.54(3)\mu_B$.

The differential behavior of both compounds can be understood by considering the electron configuration of the Mn^{3+} cations in the particular bypiramidal configuration. The splitting of the $3d$ orbitals for Mn^{3+} ions in the crystal field corresponding to the symmetry of the MnO_5 bipyramid can be deduced from the levels scheme in the paraelectric state for $YMnO_3$ above the ferroelectric Curie temperature $T_C=913$ K.[19] In the paraelectric state the space group is $P6_3/mmc$ and in the MnO_5 bipyramid the oxygens placed in the triangular basal plane are equivalent, as they are those of

the apexes.[7] The symmetry of the MnO_5 bipyramid is $\bar{6}m2$, which leads to a splitting of the $3d$ orbitals into a t_{2g} state and an e_g state. The lowest energy state, t_{2g}, is formed by a singlet, which is the ground state, plus a doublet. The highest energy state, e_g, is a doublet. Below T_C, in the ferroelectric state, the symmetry of the MnO_5 bipyramid decreases to m and both doublets split into two singlets. The relative filling of these levels by the d^4 electrons depends on the splitting of the doublets originated by the distortion of the MnO_5 bipyramid. For $YMnO_3$, Mn-O3 and Mn-O4 distances in the basal plane of the bypiramid are very different, while in $ScMnO_3$ both distances are similar. This means a greater splitting of the doublets in $YMnO_3$, which can make possible an admixture of the high spin ($S=2$) and low spin ($S=1$) states, since the lower e_g and the higher t_{2g} levels are closer. For the Sc compound, the smaller degree of distortion makes possible a predominant $t_{2g}^3\, e_g^1$ high spin ($S=2$) state.

Let us consider the magnetic interactions between Mn spins. Mn^{3+} ions are located in the (a,b) plane at 6(c) positions, forming a two-dimensional net which is perfectly triangular. In the center of each triangle there is a O^{2-} ion (O3, O4). The Mn-O-Mn bonding angle is close to 120°; therefore the indirect interaction between filled e_g states can take place via the same oxygen p orbital as well as via two perpendicular p orbitals. According to the formulation of Goodenough,[20] the superexchange interaction involves both antiferromagnetic and ferromagnetic interactions. In consequence, both types of interactions are present in the triangular spin arrangement found in these compounds. As it was indicated by Nedlin,[21] the orientation of the moments in the (a,b) plane for the $YMnO_3$ and $ScMnO_3$ magnetic structures is determined by the second-order relativistic terms. For $YMnO_3$, the Mn-O3-Mn and the Mn-O4-Mn bonding distances in the bypiramide are different, and the moments remain oriented parallel to the [120] directions in all the temperature range. For $ScMnO_3$ the Mn-O3-Mn and the Mn-O4-Mn distances are similar, and the moments that are initially parallel to the [100] directions, rotate and tend to be orientated towards the [120] direction as temperature decreases, below 75 K. Probably, the differences in the Mn-O-Mn bonding distances become significant at lower temperatures, which gives rise to a change in the direction of the easy axis.

According to Moriya,[18] two mechanisms can be responsible for the appeareance of weak ferromagnetism: the antisymmetric part of the anisotropic superexchange interaction or the magnetocrystalline anisotropy. In $ScMnO_3$ the magnetic moments are placed in the (a,b) plane; therefore the easy axis is contained in this plane. If the magnetocrystalline anisotropy was the origin of the weak ferromagnetism, as it happens in $NiFe_2$ (Ref. 18) and Mn_3Sn,[22] the spin canting would originate a distortion of the magnetic structure in order to decrease the anisotropy energy and the ferromagnetic component would appear in some direction in the (a,b) plane. However the ferromagnetic component is only possible along the z direction; in consequence we believe that the weak ferromagnetism observed in $ScMnO_3$ is originated by the antisymmetric part of the anisotropic superexchange interaction, as in α-Fe_2O_3.[18]

V. CONCLUSION

Magnetic and specific-heat measurements show that $YMnO_3$ and $ScMnO_3$ become magnetically ordered below $T_N \approx 70$ K and $T_N \approx 129$ K, respectively. The Sc compound undergoes a second magnetic transition at around 50 K; a weak ferromagnetism effect is observed in the whole ordered region. NPD data allowed us to unambiguously determine their magnetic structures. Both compounds adopt a triangular magnetic structure with the moments in the (a,b) plane, showing an antiferromagnetic coupling of the $z=0$ and $z=\frac{1}{2}$ layers. In $YMnO_3$, the Mn^{3+} moments are perpendicular to the [100] axes, and this structure is stable down to $T=1.7$ K. In contrast, in the Sc compound the spins are parallel to the [100] axes, immediately below T_N, but there is a reorientation of the magnetic moments in the basal plane at temperatures lower than 75 K, due to a variation in the magnetic anisotropy with temperature. The weak ferromagnetism observed in $ScMnO_3$ in the ordered region is believed to be of Dzialoshinskii-Moriya type, and its origin is associated with the antisymmetric part of the anisotropic superexchange interaction. Polarized neutron-diffraction experiments would be necessary to confirm that the weak ferromagnetism is directed along the [001] axis.

APPENDIX: DESCRIPTION OF THE POSSIBLE MAGNETIC STRUCTURES BASED ON GROUP THEORY

The possible magnetic structures compatible with the crystal symmetry are obtained by applying the representation theory described by Bertaut.[23] Both $YMnO_3$ and $ScMnO_3$ have the crystallographic space group $P6_3cm$, and in both cases only Mn atoms have a magnetic moment. As the propagation vector is $\boldsymbol{k}=0$ for both compounds, the theoretical treatment by group theory is the same in both cases.

For $\boldsymbol{k}=0$ the little group $G_{\boldsymbol{k}}$ coincides with the space group $P6_3cm$. According to Kovalev,[24] the irreducible representations of $G_{\boldsymbol{k}}$ are those shown in Table IV. Γ_1, Γ_2, Γ_3, and Γ_4 are unidimensional representations whereas Γ_5 and Γ_6 are two-dimensional representations. A representation Γ with the Fourier components $\boldsymbol{m}_{i\alpha}^{\boldsymbol{k}}$ ($i=1,2,\ldots,6$; $\alpha=x,y,u,z$) corresponding to the Mn atoms is then constructed. As the primitive cell is hexagonal, it is convenient to write $\boldsymbol{m}_{\boldsymbol{i}}^{\boldsymbol{k}}$ in terms of the unitary vectors $\boldsymbol{e_x}$, $\boldsymbol{e_y}$ and $\boldsymbol{e_z}$ that define the hexagonal unit cell plus the unitary vector $\mathbf{e_u}$ (where $\boldsymbol{e_u}=-\boldsymbol{e_x}-\boldsymbol{e_y}$):

$$\boldsymbol{m}_{\boldsymbol{i}}^{\boldsymbol{k}}=m_{ix}^{k}\boldsymbol{e_x}+m_{iy}^{k}\boldsymbol{e_y}+m_{iu}^{k}\boldsymbol{e_u}+m_{iz}^{k}\boldsymbol{e_z}, \tag{A1}$$

where m_{ix}^{k}, m_{iy}^{k}, and m_{iu}^{k} verify the relation: $m_{ix}^{k}+m_{iy}^{k}+m_{iu}^{k}=0$. The value of the magnetic moment for the atom i is

$$\boldsymbol{m_i}=\boldsymbol{m}_{\boldsymbol{i}}^{\boldsymbol{k}}+\boldsymbol{m_i}^{-\boldsymbol{k}}; \quad \text{with } (\boldsymbol{m}_{\boldsymbol{i}}^{\boldsymbol{k}})^{\star}=\boldsymbol{m_i}^{-\boldsymbol{k}}. \tag{A2}$$

The decomposition of Γ in terms of the irreducible representations of $G_{\boldsymbol{k}}$ is

$$\Gamma=\Gamma_1+2\Gamma_2+2\Gamma_3+\Gamma_4+3\Gamma_5+3\Gamma_6. \tag{A3}$$

The basis vectors belonging to each irreducible representation are presented in Table V. For Γ_1 and Γ_4 the magnetic moments are in a plane perpendicular to the z axis. In both cases the Mn magnetic moments are perpendicular to the

TABLE IV. Irreducible representations of the space group $G_{\mathbf{k}}=P6_3cm$ for $\mathbf{k}=0$. The symmetry operators are given in Kovalev's notation (KV) and in a notation based in Hermann-Mauguins symbols (IT). $\omega=e^{i\pi/3}$.

KV	h_1	$h_2/(\boldsymbol{\tau}^a)$	h_3	$h_4/(\boldsymbol{\tau})$	h_5	$h_6/(\boldsymbol{\tau})$	$h_{19}/(\boldsymbol{\tau})$	h_{20}	$h_{21}/(\boldsymbol{\tau})$	h_{22}	$h_{23}/(\boldsymbol{\tau})$	h_{24}
IT	1	6^+_{3z}	3^+_z	2_{1z}	3^-_z	6^-_{3z}	$c(2x,x,z)$	$m(x,x,z)$	$c(x,2x,z)$	$m(0,y,z)$	$c(x,\bar{x},z)$	$m(x,0,z)$
Pos.	x	$x-y$	$\bar{y}$	$\bar{x}$	$\bar{x}+y$	y	x	y	$\bar{x}+y$	$\bar{x}$	$\bar{y}$	$x-y$
	y	x	$x-y$	$\bar{y}$	$\bar{x}$	$\bar{x}+y$	$x-y$	x	y	$\bar{x}+y$	$\bar{x}$	$\bar{y}$
	z	$z+\frac{1}{2}$	z	$z+\frac{1}{2}$	z	$z+\frac{1}{2}$	$z+\frac{1}{2}$	z	$z+\frac{1}{2}$	z	$z+\frac{1}{2}$	z
Γ_1	1	1	1	1	1	1	1	1	1	1	1	1
Γ_2	1	1	1	1	1	1	-1	-1	-1	-1	-1	-1
Γ_3	1	-1	1	-1	1	-1	1	-1	1	-1	1	-1
Γ_4	1	-1	1	-1	1	-1	-1	1	-1	1	-1	1
Γ_5	I	B_1	$-B_2$	$-I$	$-B_1$	B_2	A	C_1	$-C_2$	$-A$	$-C_1$	C_2
Γ_6	I	$-B_1$	$-B_2$	I	$-B_1$	$-B_2$	A	$-C_1$	$-C_2$	A	$-C_1$	$-C_2$

Where: $I=\begin{pmatrix}1&0\\0&1\end{pmatrix}$ $A=\begin{pmatrix}0&1\\1&0\end{pmatrix}$ $B_1=\begin{pmatrix}\omega&0\\0&\omega^\star\end{pmatrix}$ $B_2=\begin{pmatrix}\omega^\star&0\\0&\omega\end{pmatrix}$ $C_1=\begin{pmatrix}0&\omega\\\omega^\star&0\end{pmatrix}$ $C_2=\begin{pmatrix}0&\omega^\star\\\omega&0\end{pmatrix}$

[a] $\boldsymbol{\tau}=(0,0,\frac{1}{2})$.

[100] axes. As it can be seen in Figs. 15(a) and 15(d), for Γ_1 the magnetic coupling between the layers $z=0$ and $z=\frac{1}{2}$ is antiferromagnetic whereas for Γ_4 the coupling is ferromagnetic. For Γ_2 and Γ_3 the magnetic moments have a component in the basal plane and a component parallel to the z axis [Figs. 15(b) and 15(c)]. In both cases, the component in the basal plane is parallel to the [100] axes. For Γ_2 the coupling between the z layers is antiferromagnetic for the component

TABLE V. Basis vectors corresponding to the Mn atoms, at the site 6c. The notation for the direction is $[\boldsymbol{e}_x\boldsymbol{e}_y\boldsymbol{e}_z]$; $\boldsymbol{e}_z$ is parallel to the sixfold axis and $\boldsymbol{e}_x$ and $\boldsymbol{e}_y$ are in the basal plane, forming between them a 120° angle. $\omega=e^{i\pi/3}$.

Repres. ired.	Basis vectors	Mn1 $(x,0,0)$	Mn2 $(0,x,0)$	Mn3 $(\bar{x},\bar{x},0)$	Mn4 $(\bar{x},0,\frac{1}{2})$	Mn5 $(0,\bar{x},\frac{1}{2})$	Mn6 $(x,x,\frac{1}{2})$
Γ_1	V_1^1	$[120]$	$[\bar{2}\bar{1}0]$	$[1\bar{1}0]$	$[\bar{1}\bar{2}0]$	$[210]$	$[\bar{1}\bar{1}0]$
Γ_2	V_1^2	$[100]$	$[010]$	$[\bar{1}\bar{1}0]$	$[\bar{1}00]$	$[0\bar{1}0]$	$[110]$
	V_2^2	$[001]$	$[001]$	$[001]$	$[001]$	$[001]$	$[001]$
Γ_3	V_1^3	$[100]$	$[010]$	$[\bar{1}\bar{1}0]$	$[100]$	$[010]$	$[\bar{1}\bar{1}0]$
	V_2^3	$[001]$	$[001]$	$[001]$	$[00\bar{1}]$	$[00\bar{1}]$	$[00\bar{1}]$
Γ_4	V_1^4	$[120]$	$[\bar{2}\bar{1}0]$	$[1\bar{1}0]$	$[120]$	$[\bar{2}\bar{1}0]$	$[1\bar{1}0]$
	V_1^5	$\begin{pmatrix}[100]\\ \omega^\star[\bar{1}00]\end{pmatrix}$	$\begin{pmatrix}\omega[0\bar{1}0]\\ \omega[0\bar{1}0]\end{pmatrix}$	$\begin{pmatrix}\omega^\star[110]\\ [\bar{1}\bar{1}0]\end{pmatrix}$	$\begin{pmatrix}[100]\\ \omega^\star[\bar{1}00]\end{pmatrix}$	$\begin{pmatrix}\omega[0\bar{1}0]\\ \omega[0\bar{1}0]\end{pmatrix}$	$\begin{pmatrix}\omega^\star[110]\\ [\bar{1}\bar{1}0]\end{pmatrix}$
Γ_5	V_2^5	$\begin{pmatrix}[010]\\ \omega^\star[110]\end{pmatrix}$	$\begin{pmatrix}\omega[110]\\ \omega[\bar{1}00]\end{pmatrix}$	$\begin{pmatrix}\omega^\star[\bar{1}00]\\ [010]\end{pmatrix}$	$\begin{pmatrix}[010]\\ \omega^\star[110]\end{pmatrix}$	$\begin{pmatrix}\omega[110]\\ \omega[\bar{1}00]\end{pmatrix}$	$\begin{pmatrix}\omega^\star[\bar{1}00]\\ [010]\end{pmatrix}$
	V_3^5	$\begin{pmatrix}[001]\\ \omega^\star[00\bar{1}]\end{pmatrix}$	$\begin{pmatrix}\omega[00\bar{1}]\\ \omega[00\bar{1}]\end{pmatrix}$	$\begin{pmatrix}\omega^\star[00\bar{1}]\\ [001]\end{pmatrix}$	$\begin{pmatrix}[00\bar{1}]\\ \omega^\star[001]\end{pmatrix}$	$\begin{pmatrix}\omega[001]\\ \omega[001]\end{pmatrix}$	$\begin{pmatrix}\omega^\star[001]\\ [00\bar{1}]\end{pmatrix}$
	V_1^6	$\begin{pmatrix}[100]\\ \omega^\star[100]\end{pmatrix}$	$\begin{pmatrix}\omega[0\bar{1}0]\\ \omega[010]\end{pmatrix}$	$\begin{pmatrix}\omega^\star[110]\\ [110]\end{pmatrix}$	$\begin{pmatrix}[\bar{1}00]\\ \omega^\star[\bar{1}00]\end{pmatrix}$	$\begin{pmatrix}\omega[010]\\ \omega[0\bar{1}0]\end{pmatrix}$	$\begin{pmatrix}\omega^\star[\bar{1}\bar{1}0]\\ [\bar{1}\bar{1}0]\end{pmatrix}$
Γ_6	V_2^6	$\begin{pmatrix}[010]\\ \omega^\star[\bar{1}\bar{1}0]\end{pmatrix}$	$\begin{pmatrix}\omega[110]\\ \omega[110]\end{pmatrix}$	$\begin{pmatrix}\omega^\star[\bar{1}00]\\ [0\bar{1}0]\end{pmatrix}$	$\begin{pmatrix}[0\bar{1}0]\\ \omega^\star[110]\end{pmatrix}$	$\begin{pmatrix}\omega[\bar{1}\bar{1}0]\\ \omega[\bar{1}00]\end{pmatrix}$	$\begin{pmatrix}\omega^\star[100]\\ [010]\end{pmatrix}$
	V_3^6	$\begin{pmatrix}[001]\\ \omega^\star[001]\end{pmatrix}$	$\begin{pmatrix}\omega[00\bar{1}]\\ \omega[001]\end{pmatrix}$	$\begin{pmatrix}\omega^\star[00\bar{1}]\\ [00\bar{1}]\end{pmatrix}$	$\begin{pmatrix}[001]\\ \omega^\star[001]\end{pmatrix}$	$\begin{pmatrix}\omega[00\bar{1}]\\ \omega[001]\end{pmatrix}$	$\begin{pmatrix}\omega^\star[00\bar{1}]\\ [00\bar{1}]\end{pmatrix}$

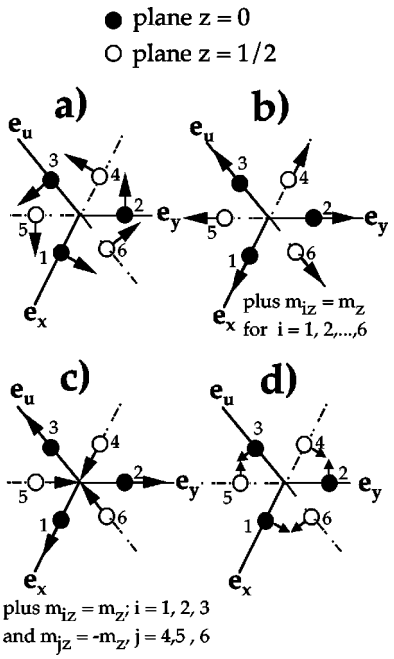

FIG. 15. Magnetic structures for $R\mathrm{MnO_3}$ associated to the unidimensional irreducible respresentations. (a) For Γ_1, (b) for Γ_2, (c) for Γ_3, (d) for Γ_4.

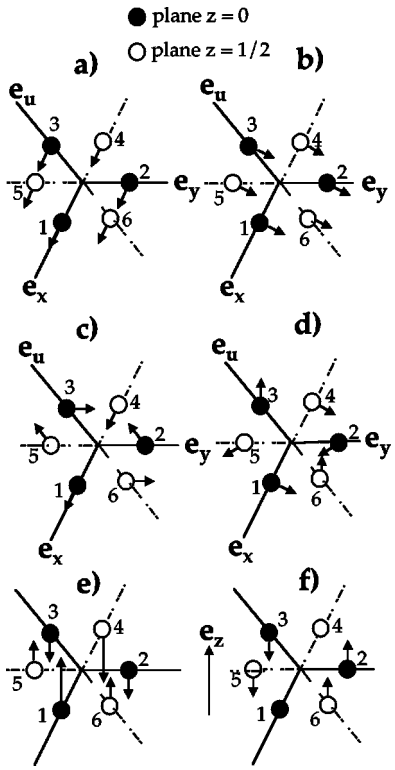

FIG. 16. Magnetic structures for $R\mathrm{MnO_3}$ associated with the bidimensional irreducible representation Γ_5. (a) Ferromagnetic with $\boldsymbol{m}_i \| [100]$. (b) Ferromagnetic with $\boldsymbol{m}_i \| [120]$. (c) $\boldsymbol{m}_1 \| [100]$. (d) $\boldsymbol{m}_1 \| [120]$. (e) and (f) solutions with nonequal moment parallel to the z axis.

in the (x,y) plane and ferromagnetic for the component along the z axis. On the contrary, for Γ_3, the coupling between the z layers is ferromagnetic for the component in the basal plane and ferromagnetic for the z component.

As Γ_5 and Γ_6 are two dimensional and complex representations the orientations of the magnetic moments cannot be obtained in a direct way. The magnetic modes will be obtained by following the procedure given by Bertaut in Ref. 25. For instance, for Γ_5, the Fourier components $\boldsymbol{m}_i^k$ can be written as a linear combination of the basis functions given in Table V as

$$\boldsymbol{m}_1^k = V_{1x}^5 \boldsymbol{e}_x + V_{1y}^5 \boldsymbol{e}_y + V_{1u}^5 \boldsymbol{e}_u + V_{1z}^5 \boldsymbol{e}_z, \tag{A4a}$$

$$\boldsymbol{m}_2^k = -\omega^\star V_{1u}^5 \boldsymbol{e}_x - \omega^\star V_{1x}^5 \boldsymbol{e}_y - \omega^\star V_{1y}^5 \boldsymbol{e}_u - \omega^\star V_{1z}^5 \boldsymbol{e}_z, \tag{A4b}$$

$$\boldsymbol{m}_3^k = -\omega V_{1y}^5 \boldsymbol{e}_x - \omega V_{1u}^5 \boldsymbol{e}_y - \omega V_{1x}^5 \boldsymbol{e}_u - \omega V_{1z}^5 \boldsymbol{e}_z, \tag{A4c}$$

$$\boldsymbol{m}_4^k = V_{1x}^5 \boldsymbol{e}_x + V_{1y}^5 \boldsymbol{e}_y + V_{1u}^5 \boldsymbol{e}_u - V_{1z}^5 \boldsymbol{e}_z, \tag{A4d}$$

$$\boldsymbol{m}_5^k = -\omega^\star V_{1u}^5 \boldsymbol{e}_x - \omega^\star V_{1x}^5 \boldsymbol{e}_y - \omega^\star V_{1y}^5 \boldsymbol{e}_u + \omega^\star V_{1z}^5 \boldsymbol{e}_z, \tag{A4e}$$

$$\boldsymbol{m}_6^k = -\omega V_{1y}^5 \boldsymbol{e}_x - \omega V_{1u}^5 \boldsymbol{e}_y - \omega V_{1x}^5 \boldsymbol{e}_u + \omega V_{1z}^5 \boldsymbol{e}_z, \tag{A4f}$$

where $V_{1\alpha}^5 = V_{11\alpha}^5/6; (\alpha = x,y,u,z)$. The function V_{11u} has been obtained after applying the projection operator method to the Fourier component m_{iu}^k, parallel to the direction $\boldsymbol{e}_u$. It is verified $V_{11u}^5 = -(V_{11x}^5 + V_{11y}^5)$. In general, the relations given in Eqs. (A4) lead to a magnetic structure with nonequal moment for the different Mn atoms. However, first we will look for solutions with equal moduli. Thus we establish the condition that $\boldsymbol{m}_i^2$ takes the same value for all the Mn atoms. It implies

$$(V_{1x}^5)^2 + (V_{1y}^5)^2 + (V_{1u}^5)^2 + (V_{1z}^5)^2 = 0, \tag{A5a}$$

$$V_{1x}^5 V_{1y}^5 + V_{1x}^5 V_{1u}^5 + V_{1y}^5 V_{1u}^5 = 0. \tag{A5b}$$

As $V_{1x}^5 + V_{1y}^5 + V_{1u}^5 = 0$, the Eqs. (A5) transform into

$$(V_{1z}^5)^2 = 0, \tag{A6a}$$

$$(V_{1x}^5)^2 + (V_{1y}^5)^2 + V_{1x}^5 V_{1y}^5 = 0. \tag{A6b}$$

Equation (A6a) implies that the magnetic moment lie in the (x,y) plane and according to Eq. (A4) the coupling between the layers $z=0$ and $z=\frac{1}{2}$ is ferromagnetic. To solve Eq. (A6b) let us put $V_{1y}^5 = \alpha V_{1x}^5$. Then, two solutions are possible: the first one is $\alpha = -\omega^\star$ and the second one is $\alpha = -\omega$. On the one hand, if $\alpha = -\omega^\star$, we obtain

$$\boldsymbol{m}_1^k = V_{1x}^5 (\boldsymbol{e}_x + \varepsilon \boldsymbol{e}_y + \varepsilon^\star \boldsymbol{e}_u); \text{ with } \boldsymbol{m}_i^k = \boldsymbol{m}_1^k \ i = 2,3,\ldots,6, \tag{A7}$$

where $\varepsilon = \omega^2 = e^{2\pi i/3}$. This solution corresponds to a ferromagnetic spin arrangement with the magnetic moments in the basal plane. In case V_{1x}^5 is real the magnetic moments are oriented parallel to the [100] direction [Fig. 16(a)] and along the [120] direction if V_{1x}^5 is purely imaginary [Fig. 16(b)]. On the other hand, if $\alpha = -\omega$, it results in

TABLE VI. Magnetic structures exhibiting weak ferromagnetism of Dzialoshinskii-Moriya type. Note: Those elements with the superscript $'$ are multiplied by the time-reversal symmetry element.

Repres.	Configuration	Ferromagnetic components	Symmetry elements
Γ_2	$\boldsymbol{m_1}=m_o\boldsymbol{e_x};\boldsymbol{m_2}=m_o\boldsymbol{e_y};\boldsymbol{m_3}=m_o\boldsymbol{e_u}$ $\boldsymbol{m_{i+3}}=-\boldsymbol{m_i}$	$\parallel[001]$	$6_3c'm'$
Γ_5	$\boldsymbol{m_1}=-2\boldsymbol{m_2}=-2\boldsymbol{m_3}=m_0\boldsymbol{e_z}$ $\boldsymbol{m_{i+3}}=-\boldsymbol{m_i}$	$\parallel[100]$	$1,2'_{1z},c(x,2x,z),m'(x,0,z)$
Γ_5	$\boldsymbol{m_1}=0;\boldsymbol{m_2}=-\boldsymbol{m_3}=m_0\boldsymbol{e_z}$ $\boldsymbol{m_{i+3}}=-\boldsymbol{m_i}$	$\parallel[120]$	$1,2'_{1z},c'(x,2x,z),m(x,0,z)$
Γ_5	$\boldsymbol{m_1}=m_o\boldsymbol{e_x};\boldsymbol{m_2}=m_o\boldsymbol{e_u};\boldsymbol{m_3}=m_o\boldsymbol{e_y}$ $\boldsymbol{m_{i+3}}=\boldsymbol{m_i}$	$\parallel[100]$	$1,2'_{1z},c(x,2x,z),m'(x,0,z)$
Γ_5	$\boldsymbol{m_1}=\frac{m_o}{\sqrt{2}}(\boldsymbol{e_y}-\boldsymbol{e_u});\boldsymbol{m_2}=\frac{m_o}{\sqrt{2}}(\boldsymbol{e_x}-\boldsymbol{e_y})$ $\boldsymbol{m_3}=\frac{m_o}{\sqrt{2}}(\boldsymbol{e_u}-\boldsymbol{e_x});\boldsymbol{m_{i+3}}=\boldsymbol{m_i}$	$\parallel[120]$	$1,2'_{1z},c'(x,2x,z),m(x,0,z)$

$$\boldsymbol{m_1^k}=V_{1x}^5(\boldsymbol{e_x}+\varepsilon^\star\boldsymbol{e_y}+\varepsilon\boldsymbol{e_u})$$

$$\text{and}\quad \boldsymbol{m_2^k}=\varepsilon^\star\boldsymbol{m_1^k};\boldsymbol{m_3^k}=\varepsilon\boldsymbol{m_1^k};$$

$$\boldsymbol{m_{3+i}^k}=\boldsymbol{m_i^k}\quad \text{for}\quad i=1,2,3. \tag{A8}$$

This solution corresponds to a triangular spin arrangement in the (x,y) plane. The magnetic moment of the Mn atoms 2 and 3, $\boldsymbol{m_2}$ and $\boldsymbol{m_3}$ are obtained by rotating by $-120°$ and 120° angle the magnetic moment $\boldsymbol{m_1}$, respectively, around the z axis. The coupling between the layers $z=0$ and $z=\frac{1}{2}$ is ferromagnetic. In case V_{1x}^5 is real or purely imaginary, the magnetic moments are orientated along specific directions. So, $\boldsymbol{m_1}$ is parallel to the [100] direction for V_{1x}^5 real [Fig. 16(c)] and parallel to the [120] direction for V_{1x}^5 purely imaginary [Fig. 16(d)].

It is worth pointing out that the equal moment condition implies that $(\boldsymbol{m_i^k})^2=(\boldsymbol{m_i}^{-\boldsymbol{k}})^2=0$. It means, if the expression given for the magnetic moment in Eq. (A2) is considered, that

$$\boldsymbol{m_i}^2=2\boldsymbol{m_i^k}\cdot\boldsymbol{m_i}^{-\boldsymbol{k}}. \tag{A9}$$

According to Eq. (A2), $\boldsymbol{m_i}$ splits into two conjugate vectors: $\boldsymbol{m_i^k}$ that belongs to the irreducible representation Γ^5 and $\boldsymbol{m_i^{-k}}$ to the $(\Gamma^5)^\star$. So Eq. (A9) is in agreement with the fact that it is only possible to construct an effective spin Hamiltonian of order 2, invariant under a group $G_{\boldsymbol{k}}$, as products of two basis vectors belonging to the same real or to two conjugate complex representations.[26]

According to Eq. (A3) the irreducible representation Γ^5 appears three times, as it is bidimensional there must be six magnetic modes associated to it. The equal module condition allowed us to find out four magnetic modes, so the another two modes must correspond to nonequal module solutions. As it can be seen in Eq. (A4), the Fourier components along the z axis, m_{iz}^k, are only given in terms of the basis function V_3^5. So if it is assumed that the magnetic moment is parallel to the z direction, the Fourier components are

$$m_{1z}^k=V_{1z}^5;\quad m_{2z}^k=-\omega^\star V_{1z}^5;\quad m_{3z}^k=-\omega V_{1z}^5;$$

$$\text{and}\quad m_{(i+3)z}^k=-m_{(i)z}^k,\quad \text{for}\quad i=1,2,3. \tag{A10}$$

In this case the coupling between the $z=0$ and $z=\frac{1}{2}$ planes is antiferromagnetic. The magnetic moment along the z direction is

$$m_{iz}=m_{1z}^k+(m_{1z}^k)^\star. \tag{A11}$$

In case V_{1z} is real the solution corresponds to $m_{1z}=-2m_{2z}=-2m_{3z}$ [Fig. 16(e)] and if V_{1z} is purely imaginary to $m_{1z}=0;\ m_{2z}=-m_{3z}$ [Fig. 16(f)].

Regarding the possible magnetic modes associated to Γ_6, these can be obtained following a similar procedure as with Γ_5. The six magnetic modes belonging to the Γ_6 are equivalent to those of Γ_5: the orientation of the magnetic moments in the $z=0$ layer is the same, but the coupling between $z=0$ and $z=\frac{1}{2}$ layers is different; for the modes with equal magnetic moment, the coupling between them is antiferromagnetic and for the mode with nonequal magnetic moment the coupling is ferromagnetic.

The different magnetic modes obtained here by the group theory representation coincides with the configurations calculated by Nedlin[21] using a thermodynamic method. In the thermodynamic potential, besides including invariants associated to the exchange interaction, terms corresponding to anisotropic relativistic interactions were taken into account.

Finally, once all the possible magnetic modes are known, it can be determined in a direct way which solutions are able to originate weak ferromagnetism of the Dzialoshinskii-Moriya type [18]. From a symmetry point of view, weak ferromagnetism is possible when a small deviation of the spins from their original direction that gives rise to a ferromagnetic component, does not change the symmetry of the magnetic structure. It means that the magnetic space group remains the same. The magnetic modes for which weak ferromagnetism is possible are presented in Table VI.

*Corresponding author. Electronic address: amunoz@elrond.uc3m.es

[1] M.A. Gilleo, Acta Crystallogr. **10**, 161 (1957).
[2] R. von Helmolt, J. Wecker, B. Holzapfel, L. Schultz, and K. Samwer, Phys. Rev. Lett. **71**, 2331 (1993); S. Jim, T.H. Tiefel, M. McCormack, R. A. Fastnacht, R. Mamesh, and L.H. Chen, Science **264**, 413 (1994).
[3] H. Yakel, W.C. Koehler, E.F. Bertaut, and F. Forrat, Acta Crystallogr. **16**, 957 (1963).
[4] E.F. Bertaut, F. Forrat, and C.R. Fang, Acad. Sci., Paris **256**, 1958 (1963).
[5] Norifumi Fujimura, Shu-ichiro Azuma, Nobuaki Aoki, Takeshi Yoshimura, and Taichiro Ito, J. Appl. Phys. **80**, 7084 (1996).
[6] Z.J. Huang, Y. Cao, Y.Y. Sun, Y.Y. Xue, and C.W. Chu, Phys. Rev. B **56**, 2623 (1997).
[7] M.N. Iliev, H.G. Lee, V.N. Popov, M.V. Abrashev, A. Hamed, R.L. Meng, and C.W. Chu, Phys. Rev. B **56**, 2488 (1997).
[8] E.F. Bertaut and M. Mercier, Phys. Lett. **5**, 27 (1963).
[9] E.F. Bertaut, M. Mercier, and R. Pauthenet, J. Phys. (France) **25**, 550 (1964).
[10] W.C. Koehler, H.L. Yankel, E.O. Wollan, and J.W. Cable, Phys. Lett. **9**, 93 (1964).
[11] E. F. Bertaut, C. R. Hebd. Seances Acad. Sci. **252**, 76 (1961); **252**, 252 (1961); **252**, 2032 (1961); **252**, 2078 (1961); **252**, 3895 (1961); J. Phys. Radium **22**, 321 (1961).
[12] H.M. Rietveld, J. Appl. Crystallogr. **2**, 65 (1969).
[13] J. Rodríguez-Carvajal, Physica B **192**, 55 (1993).
[14] *International Tables for Crystallography*, edited by A.J.C. Wilson (Kluwer-Academic, London, 1992), Vol. C, p. 391.
[15] J.E. Greedan, M. Bieringer, J.F. Britten, D.M. Giaquinta, and H.-C. zur Loye, J. Solid State Chem. **116**, 118 (1995).
[16] M. Bieringer and J.E. Greedan, J. Solid State Chem. **143**, 132 (1999).
[17] H.W. Xu, J. Iwasaki, T. Shimizu, H. Satoh, and N. Kamegashira, J. Alloys Compd. **221**, 274 (1995).
[18] I. Dzyaloshinsky, J. Phys. Chem. Solids **4**, 241 (1958); T. Moriya, Phys. Rev. **120**, 91 (1960).
[19] D. Fröhlich, St. Leute, V.V. Pavlov, and R.V. Pisarev, Phys. Rev. Lett. **81**, 3239 (1998).
[20] J.B. Goodenough, *Magnetism and the Chemical Bond* (Interscience Publishers, New York, 1963).
[21] G.M. Nedlin, Fiz. Tverd. Tela (Leningrad) **6**, 2708 (1965) [Sov. Phys. Solid State **6**, 2156 (1965)].
[22] S. Tomiyoshi and Y. Yamaguchi, J. Phys. Soc. Jpn. **51**, 2478 (1982).
[23] E. F. Bertaut, *Magnetism*, edited by G.T. Rado and H. Shul (Academic, New York, 1963), Vol. III, Chap. 4, p. 149.
[24] O.V. Kovalev, *Representations of the Crystallograpic Space Groups*, edited by Harold T. Stokes and Dorian M. Hatch (Gordon and Breach, London, 1993).
[25] E.F. Bertaut, J. Magn. Magn. Mater. **24**, 267 (1981).
[26] E.F. Bertaut, Acta Crystallogr., Sect. A: Cryst. Phys., Diffr., Theor. Gen. Crystallogr. **A24**, 217 (1968).